Contributions of Hydration and Steric (Entropic) Pressures to the Interactions between Phosphatidylcholine Bilayers: Experiments with the Subgel Phase†

Thomas J. McIntosh*,‡ and Sidney A. Simon§

Departments of Cell Biology and Neurobiology and Anesthesiology, Duke University Medical Center, Durham, North Carolina 27710

Received March 11, 1993; Revised Manuscript Received June 1, 1993

ABSTRACT: The total repulsive interaction between electrically neutral, fluid bilayer membranes is thought to have a number of components, including a hydration pressure, due to the reorientation of water by the bilayer, and steric (entropic) pressures due to bilayer undulations, head group motion, and molecular protrusions. For fully hydrated, crystalline bilayers these three steric pressures should be relatively small, and the major repulsive pressure present should be the hydration pressure. Therefore, to isolate the contribution of hydration pressure to the total interbilayer interaction, we have measured pressure–distance data by X-ray diffraction analysis of osmotically stressed dipalmitoylphosphatidylcholine (DPPC) multilayers in the subgel phase, where wide-angle and low-angle X-ray data show the bilayers are crystalline. As applied pressure was increased from 0 to 1×10^6 dyn/cm^2, the interbilayer fluid space (d_f) decreased less than 1 Å from its value at full hydration of 8.4 Å. As the pressure was increased from 1×10^6 to 3×10^7 dyn/cm^2, d_f decreased from about 8 to 4 Å. For this range of d_f, the repulsive pressure decayed exponentially with d_f with a decay length of 1.4 Å. Further increases in applied pressure did not appreciably decrease d_f, so that there was a sharp upward break in the pressure–distance curve at an interbilayer spacing of about 3 Å. In contrast, pressure–distance relations for gel ($L_{\beta'}$) phase and liquid-crystalline (L_α) phase bilayers had much softer upward breaks at $d_f < 5$ Å and extended to larger d_f at zero applied pressure. However, the pressure–distance curves for all three phases decayed exponentially with approximately the same decay length for $4 < d_f < 8$ Å. We interpret these data to mean the following: (1) the repulsion observed for $d_f < 5$ Å is primarily a steric pressure whose range depends on head group motion; (2) the steric undulation pressure plays an important role in determining the hydration properties and the range of the total repulsive pressure for fluid membranes; (3) the same underlying mechanisms govern the repulsive pressure for all phases for $4 < d_f < 8$ Å; (4) these mechanisms include a pressure due to reorientation of water molecules; and (5) the hydration pressure component extents a maximum of about two water molecules from the bilayer surface for the subgel phase.

Many experimental studies have shown that there is a strong, short-range repulsive pressure between electrically neutral lipid bilayers (LeNeveu et al., 1976, 1977; Parsegian et al., 1979; Lis et al., 1982; McIntosh & Simon, 1986b; McIntosh et al., 1989b; Rand & Parsegian, 1989). For interbilayer separations in the range of 5–15 Å, this pressure has a magnitude of several thousand atmospheres and decays exponentially with increasing distance between bilayers with a decay length of 1–2 Å (McIntosh & Simon, 1986b; McIntosh et al., 1989b; Rand & Parsegian, 1989; Simon & McIntosh, 1989). A repulsive pressure with similar range and magnitude has also been observed between DNA helices (Rau et al., 1984; Rau & Parsegian, 1992a,b) and polysaccharide molecules (Rau & Parsegian, 1990).

The molecular origin of this repulsive interaction has been the focus of a number of experimental studies (LeNeveu et al., 1977; Parsegian et al., 1979; Marra & Israelachvili, 1985; McIntosh & Simon, 1986b; Simon & McIntosh, 1989; Rand & Parsegian, 1989) and theoretical treatments (Marcelja & Radic, 1976; Schiby & Ruckenstein, 1983; Gruen & Marcelja, 1983; Attard & Batchelor, 1988; Dzhavakhidze et al., 1988; Israelachvili & Wennerstrom, 1990, 1992). Experiments have shown that the pressure cannot be due to direct electrostatic repulsion between bilayers, since it occurs between electrically neutral and uncharged bilayers and is independent of ionic strength (LeNeveu et al., 1977; Parsegian et al., 1979; McIntosh et al., 1989c; Rand & Parsegian, 1989). Many experimental (LeNeveu et al., 1977; Parsegian et al., 1979; McIntosh et al., 1989c; Simon et al., 1991) and theoretical (Marcelja & Radic, 1976; Gruen & Marcelja, 1983; Schiby & Ruckenstein, 1983; Cevc & Marsh, 1985; Attard & Batchelor, 1988; Kornyshev & Leikin, 1989; Leikin & Kornyshev, 1990) studies have termed this interaction a "hydration pressure" or "solvation pressure", arguing that the underlying cause of the repulsion is the partial ordering or polarization of water or solvent molecules by the hydrophilic bilayer surface. Unfortunately, there is no experiemntal evidence that directly demonstrates the orientation or layering of the solvent molecules by bilayers, although NMR measurements of egg phosphatidylcholine bilayers show distinct regions of quadrupole splittings as a function of hydration (Gawrisch et al., 1988), and X-ray crystallography has shown nonrandom arrangements in water molecules that extend several layers from the surface of certain protein crystals (Badger & Caspar, 1991). Moreover, there are no theoretical models from which the magnitude and range of the hydration pressure can be calculated from first principles for a particular hydrated surface. For lipid bilayers, the magnitude of this observed pressure has been shown to be proportional to the square of the dipole potential measured in monolayers in equilibrium with liposomes, suggesting that the "hydration" pressure results, at least in part, from the polarization of interbilayer water by electric fields arising from the lipid and water dipoles (Simon & McIntosh, 1989; Simon et al., 1992).

† This work was supported by a grant from the National Institutes of Health (GM-27278).

‡ Department of Cell Biology.

§ Department of Neurobiology and Anesthesiology.

0006-2960/93/0432-8374$04.00/0

Recently, Israelachvili and Wennerstrom (1990, 1992) proposed a quite different mechanism for the origin of this short-range repulsion between bilayers. Their theory states that the pressure is of entropic origin, caused by steric interactions of "hydrocarbon chains and other parts" of the lipid molecules that protrude into the fluid space from apposing bilayer surfaces (Israelachvili & Wennerstrom, 1992).

The competing "hydration" and "protrusion" models for this short-range interaction have to a large extent been based on different interpretations of the same sets of experimental data. For example, McIntosh et al. (1989b) measured repulsive pressures between lipid bilayers formed in three solvents—water, formamide, and 1,3-propanediol. They found that the decay length of the pressure depends on the solvent, being largest for 1,3-propanediol and smallest for water. They argued that this result is consistent with the force being due to the reorientation of solvent molecules by the bilayer surface, since the measured decay length correlates with the size of the solvent molecule (McIntosh et al., 1989b). On the other hand, Israelachvili and Wennerstrom (1990, 1992) argued that these data are consistent with the protrusion model, since the range of the pressure increases with decreasing interfacial energy of the hydrocarbon–solvent interfaces. Although the protrusion model has been used to explain these data from different solvents and other data, arguments have been presented that the protrusion model is not consistent with pressure–distance data obtained from gel-phase lipids (Parsegian & Rand, 1991; McIntosh et al., 1992a) or from lipids containing cholesterol (Parsegian & Rand, 1991; McIntosh et al., 1992a) or cholesterol analogs (Simon et al., 1992).

A complicating factor in the interpretation of much of the existing experimental data is the presence of two other repulsive pressures that contribute to the measured pressure–distance relations between fluid bilayers: the first pressure is very short-range and the second is of longer range. For the first case, McIntosh et al. (1987) found an upward break in the pressure–distance relationships for liquid-crystalline egg phosphatidylcholine (egg PC)[1] bilayers starting at an interbilayer separation of about 5 Å. They interpreted this upward break as being primarily due to the onset of steric hindrance between the flexible lipid head groups, arguing that the phosphorylcholine head groups can rotate so that they can extend 2–3 Å into the fluid space between bilayers. Israelachvili and Wennerstrom (1992) also note that an entropic pressure from "overlapping mobile headgroups" might contribute to the total short-range interaction between bilayers. In the second case, theoretical treatments (Helfrich, 1973; Evans & Parsegian, 1986; Evans & Needham, 1987; Podgornik & Parsegian, 1992) have predicted the presence of a relatively long-range entropic pressure between liquid-crystalline bilayers, caused by thermally driven mechanical fluctuations or undulations of the entire bilayer. This fluctuation or undulation pressure has been detected in micropipet experiments of large single-walled vesicles (Evans, 1991) and in X-ray experiments of monoglyceride bilayers (McIntosh et al., 1989c) and sodium dodecyl sulfate/cosurfactant membranes in water (Safinya et al., 1989). Comparisons of X-ray data for solid and fluid monoglyceride bilayers have experimentally shown the effects of such fluctuations on pressure–distance relations (McIntosh et al., 1989c). For fluid, short chain length monoglyceride bilayers, the magnitude of the undulation pressure becomes significant compared to the hydration pressure and larger than the attractive van der Waals pressure at interbilayer spacings greater than about 10 Å, causing these bilayers to swell without limit (McIntosh et al., 1989c).

In this article, our goal is to obtain further data for phospholipid bilayers that will help distinguish the interbilayer pressure due to orientation of water molecules from the various steric pressures due to lipid head group motion, lipid protrusions, and bilayer fluctuations. We do this by measuring pressure–distance data from the "subgel" phase of phosphatidylcholine and comparing these data to similar data from gel ($L_{\beta'}$) and liquid-crystalline (L_α) phosphatidylcholine bilayers (McIntosh et al., 1987; McIntosh & Simon, 1986b). For hydrated dipalmitoylphosphatidylcholine (DPPC) bilayers, the subgel phase is formed after incubation of hydrated DPPC for several days at temperatures near 0 °C (Chen et al., 1980; Ruocco & Shipley, 1982a,b; Tristam-Nagle et al., 1987). The transition from the subgel to gel phase of DPPC occurs between 13 and 18 °C, depending on the scanning rate (Chen et al., 1980; Tristam-Nagle et al., 1987). The rationale for our experiments is that the motion of both the lipid head group and the hydrocarbon chains is considerably reduced in the subgel phase as compared to either gel or liquid-crystalline phases. Nuclear magnetic resonance experiments show that, at least on the NMR time scale, the head group and chains are relatively immobile in the subgel phase (Akutsu, 1986). In fact, Akutsu et al. (1986) note that "...the rotational motion of the polar headgroup is so restricted in the subgel phase that it cannot average out the chemical-shift anisotropy around the rotational axis." In addition, wide-angle X-ray diffraction data show that the entire DPPC molecule is crystallized in the subgel phase (Ruocco & Shipley, 1982a,b). Therefore, since the acyl chains are crystallized and the head group motions are severely restricted in the subgel phase, one would expect that head group motions, molecular protrusions, and bilayer undulations should be dramatically reduced in the subgel phase as compared with gel and especially liquid-crystalline phases.

An additional reason to measure the repulsive pressure between subgel bilayers is that it provides a test of recent theoretical treatments of the hydration pressure (Kornyshev & Leikin, 1989; Leikin & Kornyshev, 1991; Kornyshev et al., 1992) that predict that the decay length of the hydration pressure should depend on the degree of ordering of the head groups in the bilayer. That is, these theories predict that the more ordered the dipoles in the head group region, the smaller the decay length.

We use X-ray diffraction analysis of osmotically stressed bilayers to obtain pressure–distance relations for subgel DPPC bilayers. These data, along with corresponding pressure–distance data from gel ($L_{\beta'}$) and liquid-crystalline (L_α) bilayers, are modeled in terms of van der Waals attractive and steric and hydration repulsive interactions.

MATERIALS AND METHODS

Dipalmitoylphosphatidylcholine (DPPC) was purchased from Avanti Polar Lipids, and poly(vinylpyrrolidone) (PVP) with an average molecular weight of 40 000 was purchased from Sigma Chemical Co.

Two types of lipid systems were examined by X-ray diffraction: unoriented suspensions of multiwalled DPPC vesicles and oriented DPPC multilayers. Known osmotic pressures were applied to both of these systems by published procedures (LeNeveu et al., 1977; Parsegian et al., 1979; McIntosh & Simon, 1986a; McIntosh et al., 1987). Osmotic stress was applied to the DPPC liposomes by incubating them in aqueous solutions of the neutral polymer PVP. Since this

[1] Abbreviations: DPPC, dipalmitoylphosphatidylcholine; egg PC, phosphatidylcholine from egg yolks; PVP, poly(vinylpyrrolidone).

polymer is too large to enter the lipid lattice, it competes for water with the DPPC multilayers, thereby applying an osmotic pressure (LeNeveu et al., 1976, 1977). Osmotic pressures for the PVP solutions were calculated from the virial coefficients of Vink (1971). These values are in close agreement with values measured by McIntosh et al. (1989b). Pressure was applied to the oriented DPPC multibilayers by incubating them in constant relative humidity atmospheres maintained with saturated salt solutions. The ratio of the vapor pressure (p) of various salt solutions to the vapor pressure of pure water (p_0) has been determined (O'Brien, 1948; Weast, 1984). The applied pressure is given by

$$P = -(RT/V_w) \ln (p/p_0) \quad (1)$$

where R is the molar gas constant, T is the temperature in kelvin, and V_w is the partial molar volume of water (Parsegian et al., 1979).

The DPPC suspensions were formed by adding 5 mg of DPPC to 500 μL of the appropriate polymer solution and allowing the mixture to incubate for several hours at 60 °C, a temperature above the main phase transition temperature of DPPC. The subgel phase was formed by keeping the specimens at 2 °C for at least 15 days. Specimens that were incubated at 2 °C for 3 months gave diffraction patterns identical to those of samples that were incubated for 15 days. The multilamellar lipid vesicles were concentrated by centrifugation with a bench centrifuge at 2 °C, sealed in quartz capillary tubes, and mounted in a temperature-regulated specimen holder on a point collimation X-ray camera. X-ray patterns from these unoriented dispersions in the subgel phase were collected at 10 °C. Oriented multilayers of DPPC in the subgel phase were formed by placing a small drop of DPPC–water suspension, previously hydrated at 60 °C, onto a curved glass substrate and incubating for 15 days at 2 °C in a chamber with controlled relative humidity atmosphere. Constant relative vapor pressures (p/p_0) were maintained by use of saturated salt solutions (O'Brien, 1948), as described previously (McIntosh et al., 1987, 1989a). The multilayers on the glass substrate were mounted in a controlled humidity chamber on a single-mirror (line-focused) X-ray camera such that the X-ray beam was oriented at a grazing angle relative to the multilayers (McIntosh et al., 1987, 1989a). The humidity chamber, which contained a cup of the appropriate saturated salt solution, consisted of a hollow-walled copper cannister with two Mylar windows for passage of the X-ray beam. To speed equilibration, a very gentle stream of nitrogen was passed through a flask of the saturated salt solution and then through the chamber. The temperature within the humidity chamber was controlled by means of water circulating through the copper canister. The flask of the saturated salt solution was maintained at the same temperature as the specimen chamber. X-ray diffraction patterns from oriented multilayers were recorded for specimens at two temperatures, 10 and 20 °C.

For both oriented and unoriented specimens, X-ray diffraction patterns were recorded on Kodak DEF X-ray film. X-ray films were processed by standard techniques and densitometered with a Joyce-Loebl microdensitometer as described previously (McIntosh & Simon, 1986b; McIntosh et al., 1987, 1989a, 1992b). After background subtraction, integrated intensities, $I(h)$, were obtained for each order h by measuring the area under each diffraction peak. For unoriented patterns, the structure amplitude, $F(h)$, was set equal to $\{h^2 I(h)\}^{1/2}$ (Blaurock & Worthington, 1966; Herbette et al., 1977). For the oriented line-focused patterns, the intensities were corrected by a single factor of h due to the cylindrical curvature of the multilayers (Blaurock & Worthington, 1966; Herbette et al., 1977), so that $F(h) = \{hI(h)\}^{1/2}$.

Electron density profiles, $\rho(x)$, on a relative electron density scale were calculated from

$$\rho(x) = (2/d) \sum \exp\{i\phi(h)\} F(h) \cos (2\pi x h/d) \quad (2)$$

where x is the distance from the center of the bilayer, d is the lamellar repeat period, $\phi(h)$ is the phase angle for order h, and the sum is over h. Phase angles were determined by the use of the sampling theorem (Shannon, 1949) as described in detail previously (McIntosh & Simon, 1986b; McIntosh & Holloway, 1987). Most electron density profiles described in this article are at a resolution of $d/2h_{max} \approx 7$ Å, with the exception of the profiles in Figure 5C which are at a resolution of $d/2h_{max} \approx 3.5$ Å.

RESULTS

For all oriented and unoriented DPPC specimens at both 10 and 20 °C, the X-ray diffraction patterns consisted of a series of low-angle reflections, which indexed as orders of a lamellar repeat period, and several wide-angle reflections. For samples at 10 °C that had previously been incubated at 2 °C (see Materials and Methods), the most intense wide-angle reflections were a sharp reflection at 4.4 Å and a broader reflection centered at 3.9 Å. Other sharp wide-angle reflections were observed at spacings of 9.8 and 6.8 Å. These reflections are characteristic of bilayers in the subgel phase (Fuldner, 1981; Ruocco & Shipley, 1982a,b). The spacings of these wide-angle reflections did not change as a function of applied osmotic pressure. However, the lamellar repeat period of DPPC in the subgel phase varied as a function of applied pressure. These data are shown in Figure 1A, which is a plot of the logarithm of applied pressure (log P) versus repeat period. The lamellar repeat period for DPPC in the subgel phase in excess water (no applied osmotic pressure, indicated by the arrow in Figure 1A) was 59.4 Å, in close agreement with previous diffraction studies (Fuldner, 1981; Ruocco & Shipley, 1982a,b). As the applied pressure increased from 0 to 3×10^7 dyn/cm^2, the lamellar repeat period decreased to about 54 Å. For applied pressures from 1.0×10^8 to 1.3×10^9 dyn/cm^2, the repeat period was nearly constant, reaching a limiting value of 53.7 Å (Figure 1A).

For comparison, the same oriented DPPC multilayers were also examined after heating to 20 °C for a range of relative vapor pressures from 0.98 to 0.15. For these specimens, the wide-angle pattern consisted of a sharp reflection at 4.2 Å and a broader band at 4.1 Å, characteristic of DPPC in the gel ($L_{\beta'}$) phase (Tardieu et al., 1973). The lamellar repeat periods for these specimens as well as those previously obtained for gel-phase DPPC suspensions in PVP solutions (McIntosh & Simon, 1986b) are shown in Figure 1B. For the experiments with oriented DPPC multilayers in relative vapor pressures, the repeat periods represent mean values of 2–3 experiments, and these repeat periods are in close agreement with those obtained recently for gel-phase DPPC under similar conditions by Katsaras et al. (1992). As shown in Figure 1B, at a given applied pressure the lamellar repeat period for DPPC in the gel phase was always several angstroms larger than the repeat period for DPPC in the subgel phase. For comparison, Figure 1B also shows log P versus repeat period for egg phosphatidylcholine bilayer in the liquid-crystalline phase at 20 °C [from McIntosh et al. (1987)].

The lamellar repeat period contains the contributions of both the lipid bilayer and the fluid spacing between adjacent

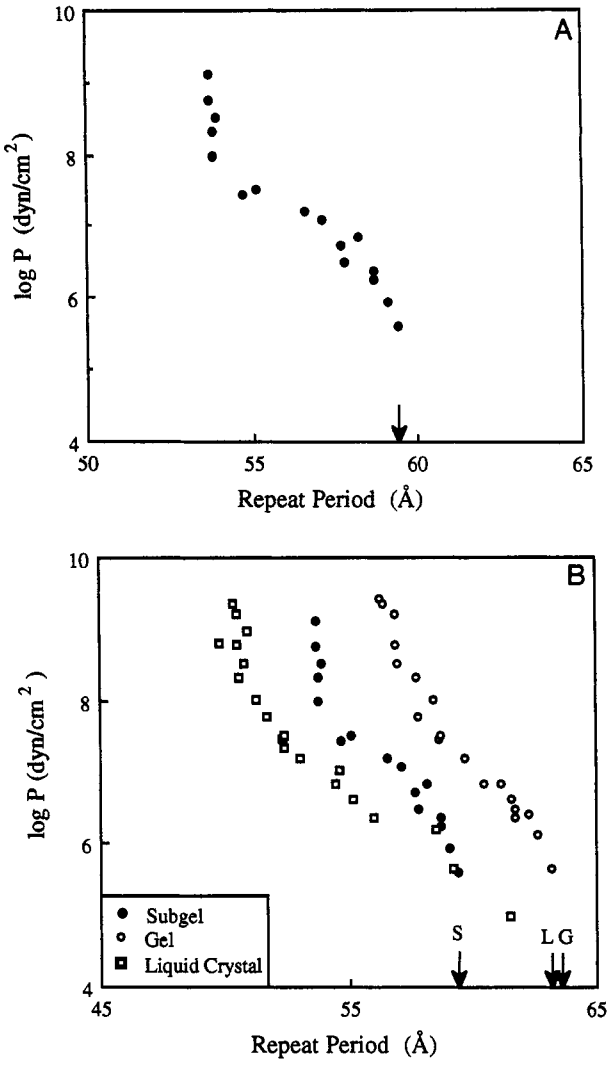

FIGURE 1: (A) Logarithm of applied pressure (log P) plotted versus the lamellar repeat period for subgel-phase DPPC bilayers. The arrow indicates the repeat period in excess water with no applied pressure. (B) log P plotted versus the lamellar repeat period for subgel-phase DPPC bilayers (●), gel-phase DPPC bilayers (○), and liquid-crystalline phase egg PC bilayers (□). The arrows indicate the repeat period in excess water for these subgel (S), gel (G), and liquid-crystalline (L) bilayers. All of the egg PC data and the DPPC data for log $P < 7.6$ are taken from McIntosh and Simon (1986b).

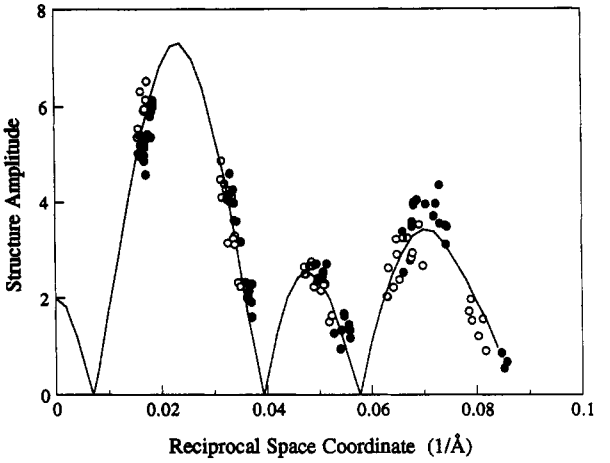

FIGURE 2: Structure amplitudes plotted versus reciprocal space coordinate for DPPC in the subgel phase (●) and gel phase (○). The solid line is the continuous transform for DPPC in the gel phase taken from Figure 1C of McIntosh and Simon (1986b).

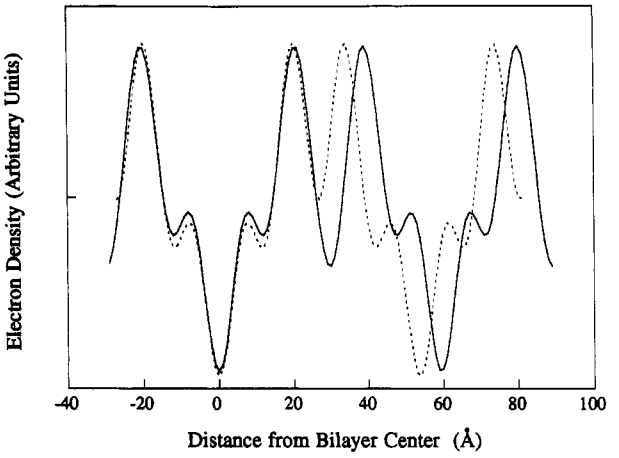

FIGURE 3: Electron density profiles for subgel DPPC bilayers in excess water (—) and with an applied pressure of 1.3×10^9 dyn/cm^2 (- - -). For each system, two adjacent bilayers are shown with the origin located at the center of the bilayer on the left. The resolution of these profiles is $d/2h_{max} \approx 7$ Å.

bilayers. Information on the thickness of both the bilayer and the fluid layer between bilayers was determined from electron density profiles obtained from the X-ray structure amplitude data (eq 2). Structure amplitudes for DPPC in both the gel and the subgel phases are plotted versus the reciprocal space coordinate in Figure 2. The structure amplitudes for these two phases all fell close to the same smooth curve, the continuous transform of the bilayer structure of fully hydrated DPPC (solid line in Figure 2). This means that (1) the phase angles were the same for the gel and subgel phases and (2) the bilayer organization of the two phases was similar. However, the structure amplitudes for DPPC in the subgel phase were slightly displaced from the continuous transform in certain regions of reciprocal space. For example, the structure amplitudes for the subgel phase fell slightly to the right of the solid line in the region of the transform near $X = 0.035$ Å^{-1} and fell slightly above the solid line near $X = 0.07$ Å^{-1}. This observation implies that the bilayer structure was slightly different in the gel and subgel phases. Differences in structure between gel and subgel phases and changes in stucture as a function of applied osmotic pressure were quantitated by the electron density profile analysis.

Figure 3 shows electron density profiles for the subgel phase at the two extremes of applied pressure, $P = 0$ dyn/cm^2 (bilayers in excess water with no applied osmotic pressure) and $P = 1.3 \times 10^9$ dyn/cm^2 (bilayers at a relative vapor pressure of 0.38). For each applied pressure, these profiles show two unit cells, with two adjacent bilayers and the interbilayer fluid space. Consider the bilayer on the left-hand side of each profile. The low-density trough in the bilayer center (at $x = 0$ Å) corresponds to the localization of the low-density terminal methyl groups in the center of the bilayer. The two electron density peaks, near ±20 Å, correspond to the DPPC head groups. The medium-density regions between the head group peaks and the terminal methyl trough correspond to the methylene chain region of the bilayer. The medium-density region between adjacent bilayers (centered near $x = 30$ Å for the profile in excess water) corresponds to the fluid space between adjacent bilayers. The profiles in Figure 3 show two important points. First, the profiles of the left-hand bilayers superimposed quite closely, meaning that, at this resolution, the bilayer structure was nearly the same over this range of applied pressure. Second, the spacing between adjacent bilayers, as indicated by the separation of

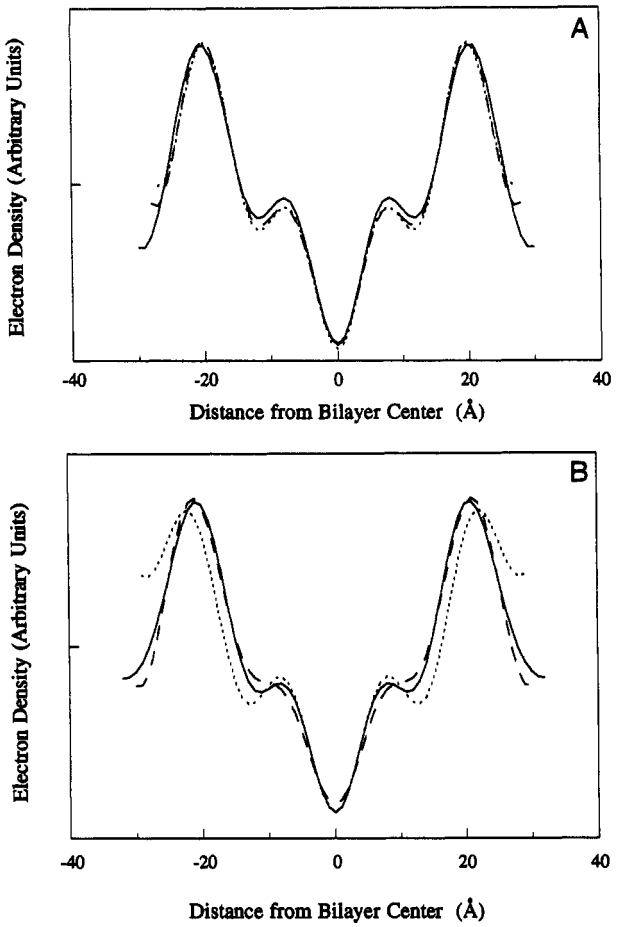

FIGURE 4: Electron density profiles showing one bilayer for (A) subgel DPPC bilayers in water (—) and at applied osmotic pressures of 2.8×10^7 dyn/cm^2 (– –) and 1.3×10^9 dyn/cm^2 (- - -) and (B) gel DPPC bilayers in water (—) and at applied osmotic pressures of 2.8×10^7 dyn/cm^2 (– –) and 1.6×10^9 dyn/cm^2 (- - -). The profile of gel-phase DPPC in water is calculated from the data of McIntosh and Simon (1986b). For all profiles, the center of the bilayer is at the origin and the resolution is $d/2h_{max} \approx 7$ Å.

head group peaks from adjacent bilayers, was decreased about 5 Å closer by an applied pressure of $P = 1.3 \times 10^9$ dyn/cm^2.

To illustrate more clearly the invariance of bilayer structure for the subgel phase with applied pressure, profiles containing one unit cell from three different osmotic pressures are shown in Figure 4A. The profiles of the subgel bilayers from the three applied pressures superimposed quite closely. There was no systematic change in bilayer thickness with increasing applied pressure in the subgel phase. To quantitate this observation, we measured the head group peak-to-head group peak separation for profiles at all osmotic pressures. The peak-to-peak separation was 41.0 ± 0.6 Å (mean ± standard deviation for $N = 15$ experiments). For the gel phase of DPPC, we (McIntosh & Simon, 1986b) have previously shown that there was no appreciable change in bilayer thickness for the range of applied pressure $0 < P < 6 \times 10^7$ dyn/cm^2. For these pressures, the peak-to-peak separation for gel-phase DPPC was 41.9 ± 0.6 Å (mean ± standard deviation, $N = 11$). However, we report here that there was a small, but reproducible, change in the bilayer thickness for gel-phase DPPC in the gel phase at pressures greater than about 1×10^9 dyn/cm^2. For experiments at these high applied pressures, the peak-to-peak spacing was 44.0 ± 0.6 Å (mean ± standard deviation, $N = 4$). This increase in bilayer thickness is shown in the profiles in Figure 4B.

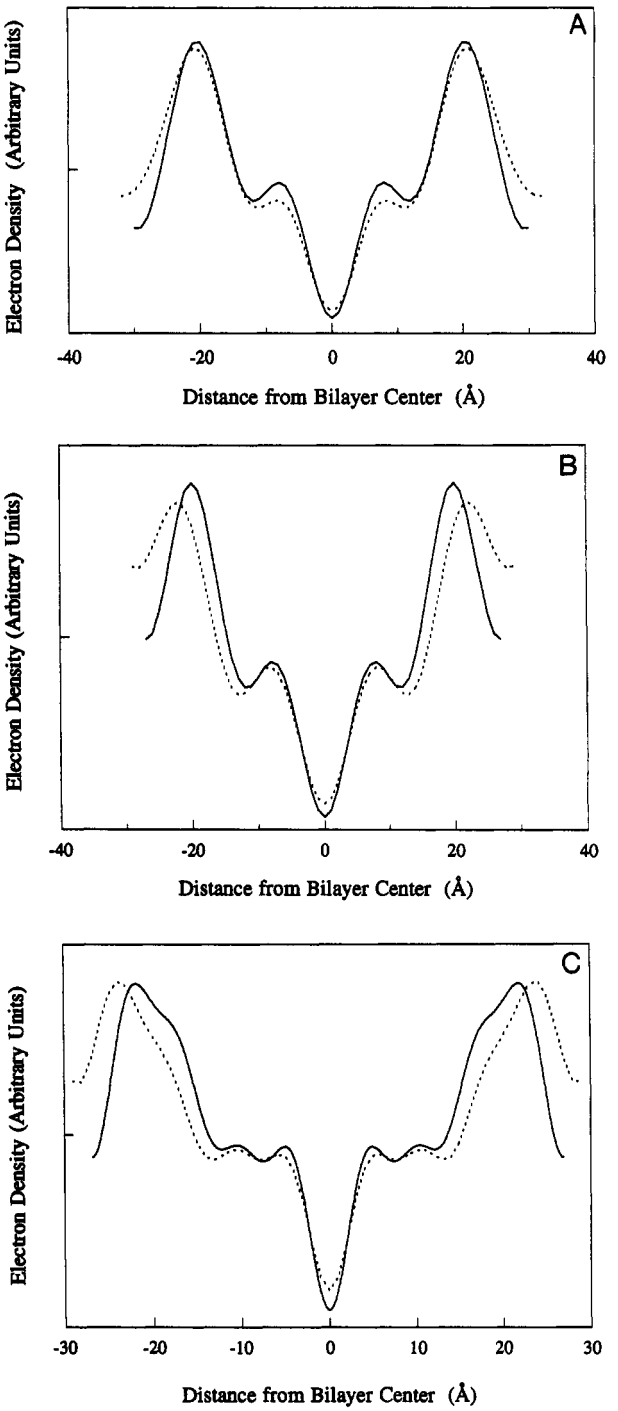

FIGURE 5: Electron density profiles showing one bilayer for (A) subgel DPPC bilayers (—) and gel DPPC bilayers (- - -) in excess water and (B and C) subgel DPPC bilayers at an applied osmotic pressure of 1.3×10^9 dyn/cm^2 (—) and gel DPPC bilayers at an applied osmotic pressure of 1.6×10^9 dyn/cm^2 (- - -). For A and B the profiles are at a resolution of $d/2h_{max} \approx 7$ Å, whereas the profiles in C are at a resolution of $d/2h_{max} \approx 3.5$ Å. For all profiles the center of the bilayer is at the origin.

Profiles at a resolution of $d/2h_{max} \approx 7$ Å for DPPC in the gel and subgel phases are compared for zero applied pressure in Figure 5A and at high applied pressures in Figure 5B. In excess water (Figure 5A), the profiles of gel and subgel DPPC were quite similar, with the gel-phase bilayer being only slightly wider. However, at high applied pressure (Figure 5B), the gel-phase bilayer was noticeably wider. For high applied pressures with long exposure times, higher resolution ($d/2h_{max} \approx 3.5$ Å) data were recorded. Figure 5C shows profiles

of gel and subgel DPPC at 3.5-Å resolution. In these profiles, the methylene chain region of the bilayers is better resolved: the head group region contains two partially resolved peaks corresponding to the phosphate moiety and the glycerol backbone (Lesslaer et al., 1972). In the profiles in Figure 5C, the width of the head group region is similar for the gel and subgel phases, although the electron density in the region between adjacent bilayers is significantly smaller for the subgel phase.

The electron density profiles can be used to estimate the distance between adjacent bilayer surfaces as a function of applied pressure. We use the profiles obtained at moderate (7 Å) resolution, since this is the best resolution obtained at low applied pressures. As noted previously (McIntosh & Simon, 1986b; McIntosh et al., 1987, 1989a, 1992a), the definition of the lipid–water interface is somewhat arbitrary, because the bilayer surface is not smooth and water penetrates into the head group region of the bilayer (Worcester & Franks, 1976; Simon et al., 1982). We use electron density profiles to estimate the physical edge of the bilayer since this method makes is possible to distinguish steric and hydration pressures (McIntosh et al., 1987). The gravimetric method (LeNeveu et al., 1977) of calculating "partial lipid" and "partial water layer" thicknesses assumes that the lipid and water form separate layers, so that, by implicit assumption, steric interactions between apposing lipid bilayers cannot be observed until all water is removed from the system. We operationally define the bilayer width as the total physical thickness of the bilayer, assuming that the conformation of the phosphorylcholine head group in subgel DPPC bilayers is the same as it is in single crystals of phosphatidylcholine (Pearson & Pascher, 1979). In that case the high-density head group peak in the 7-Å resolution profiles would be located between the phosphate group and the glycerol backbone. We assume that the phosphorylcholine group is, on average, oriented approximately parallel to the bilayer plane, so that the edge of the bilayer lies about 5 Å outward from the center of the high-density peaks in the 7-Å resolution electron density profiles (McIntosh & Simon, 1986b; McIntosh et al., 1987, 1989a, 1992a). Therefore, for each osmotic pressure we calculated the bilayer thickness as the distance between head group peaks across the bilayer in the profiles plus 10 Å. The distance between bilayer surfaces (d_f) was calculated as the difference between the lamellar repeat period and this bilayer thickness (McIntosh & Simon, 1986b; McIntosh et al., 1987, 1989a, 1992a). This same procedure was used previously to estimate the bilayer thickness and d_f for pressure–distance relations for gel-phase DPPC and liquid-crystalline egg PC (McIntosh & Simon, 1986b).

Using this definition of the lipid–water interface, we plot in Figure 6A the common logarithm of applied pressure versus the distance between bilayer surfaces for the subgel phase. As applied pressure increased from 0 to about 1×10^6 dyn/cm^2, the fluid space decreased by less than 1 Å from the equilibrium fluid separation of 8.4 Å. As the pressure was increased from 1×10^6 to 3×10^7 dyn/cm^2, the distance between bilayers decreased from over 7 to about 3 Å. As shown in our modeling studies in the Discussion, for this range of bilayer separations the data points could be fit closely with a straight line, indicating that for this range of d_f the repulsive pressure between bilayers can be described as an exponential decay such that $P = P_0 \exp(-d_f/\lambda)$. Further increases in applied pressure did not appreciably decrease the distance between bilayers. That is, there was a sharp upward break in the pressure–distance curve at an interbilayer spacing of about 3 Å.

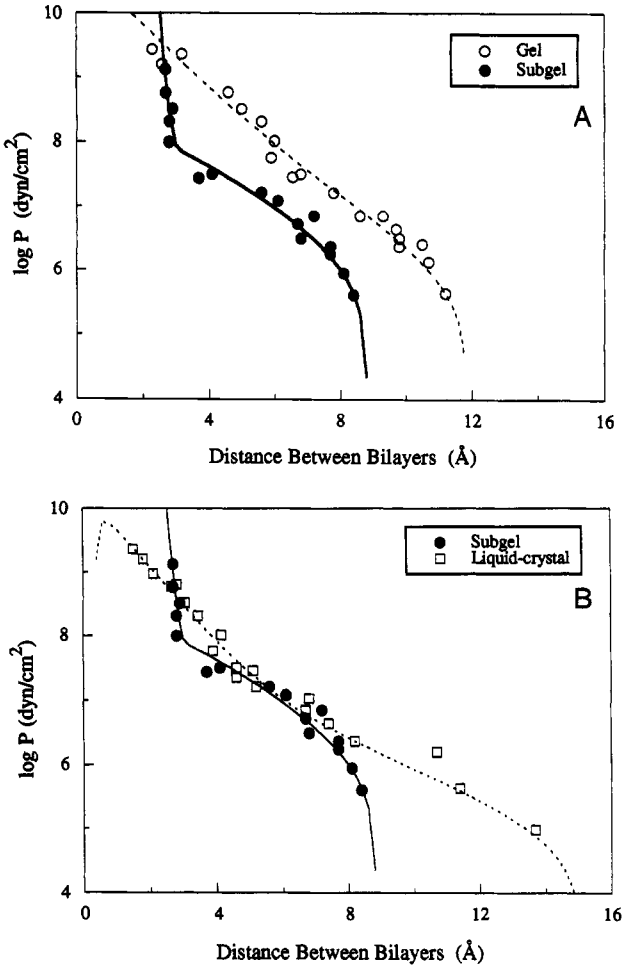

FIGURE 6: (A) Logarithm of applied pressure (log P) plotted versus the distance between bilayers (d_f) for subgel-phase DPPC (●) and gel-phase DPPC bilayers (○). The solid line is the linear least-squares fit to the subgel data ($R^2 = 0.99$) with $P = P_{vsr} + P_{sr} + P_u - P_v$, with $P_{vsr} = 5.18 \times 10^{25} \exp(-(d_f/0.07)$ dyn/cm^2, $P_{sr} = 1.11 \times 10^9 \exp(-d_f/1.43)$ dyn/cm^2, $P_u = 0$, and $P_v = -(3.0 \times 10^{10})/6\pi d_f^3$ dyn/cm^2. The dashed line represents the least-squares ($R^2 = 0.99$) fit to the gel-phase data with $P_{vsr} = 7.2 \times 10^{10} \exp(-d_f/0.80)$, $P_{sr} = 4.5 \times 10^9 \exp(-d_f/1.40)$, $P_u = 0$, and $P_v = (3.0 \times 10^{10})/6\pi d_f^3$ dyn/cm^2. (B) log P plotted versus d_f for subgel-phase DPPC bilayers (●) and liquid-crystalline egg PC bilayers (□). The solid line represents the interaction between subgel-phase bilayers and has the parameters given in Figure 6A. The dashed line represents the least-squares ($R^2 = 0.99$) fit to the liquid-crystalline data with $P = P_{vsr} + P_{sr} + P_u - P_v = 7.84 \times 10^{13} \exp(-d_f/0.68)$, $+ 4.0 \times 10^8 \exp(-d_f/1.38) + 1.28 \times 10^6 \exp(-d_f/2.76) - (2.5 \times 10^{10})/6\pi d_f^3$ dyn/cm^2.

For comparison, pressure–distance data for the subgel phase are plotted together with data from the gel phase of DPPC and the liquid-crystalline phase of egg PC in Figures 6A,B, respectively. The equilibrium fluid spaces in excess water were 8.4, 11.7, and 15.4 Å for the subgel, gel, and liquid-crystalline phases, respectively. Given that the width of a water molecule is 2.8 Å, the bilayers are separated by a fluid spacing corresponding to approximately 3, 4, and 5 water molecules for the subgel, gel, and fluid phases, respectively. For all three lipid phases, the fluid space between adjacent bilayers decreased with applied osmotic pressure. For the range $4 \leq d_f \leq 8$ Å, the three curves were approximately parallel. In this range of interbilayer distances, the subgel and liquid-crystalline bilayers had about the same pressure (Figure 6B) and the gel-phase bilayer had a larger pressure at each spacing (Figure 6A). However, the shapes of the

pressure–distance relations for the three phases were quite different for $d_f < 4$ Å and $d_f > 8$ Å. First consider the region for $d_f < 4$ Å. The upward break in the pressure–distance curve at small distances was much sharper for the subgel phase than for either the gel or liquid-crystalline phase. The upward break at about 3 Å for the subgel phase was extremely sharp (Figure 6A), whereas the previously observed (McIntosh et al., 1987) upward break in the pressure–distance curve for the liquid-crystalline phase was not as steep and extended from about 5 to about 2 Å (Figure 6B). In the case of gel-phase DPPC, the presence of a corresponding upward break in the pressure–distance relation was difficult to demonstrate. In the region of the curves for $d_f > 8$ Å, the most obvious difference was that the pressure–distance relation for the liquid-crystalline bilayers extended to larger interbilayer distances, so that the equilibrium fluid separation was considerably larger for the liquid-crystalline phase than for the subgel phase (Figure 6B).

DISCUSSION

The X-ray data presented in this article provide information on the structure of the subgel phase and also provide insights as to the relative magnitudes of the hydration and steric (entropic) forces between bilayer surfaces.

Structure and Hydration of the Subgel Phase

Previous authors (Fuldner, 1981; Ruocco & Shipley, 1982a,b) have noted the difference in low-angle and wide-angle spacings between gel ($L_{\beta'}$) and subgel phases. Hydrocarbon chain packing models have been presented to explain the origin of the two major wide-angle reflections at 4.4 and 3.9 Å (Ruocco & Shipley, 1982a,b). Our electron density profiles provide information concerning the relative thickness of the bilayer and fluid spacings in the gel and subgel phases. The X-ray analysis shows that the bilayer thickness, as measured by mean head group separation in electron density profiles (Figures 3–5), is similar for gel and subgel bilayers. The small (less than 1 Å) difference in bilayer thickness between the two phases in excess water can be explained in terms of the subgel phase having a slightly larger hydrocarbon chain tilt compared to the gel phase. This is consistent with the chain packing model of Ruocco and Shipley (1982b), which finds that the area per hydrocarbon chain (in a plane perpendicular to the chain) is slightly smaller in the subgel phase (19.0 Å^2) than in the gel phase (19.5 Å^2). A smaller area per chain would imply a larger chain tilt, since it is thought that chain tilt in DPPC bilayers in excess water is caused by the mismatch between the excluded area in the plane of the membrane of the PC head groups and the hydrocarbon chains (McIntosh, 1980). Assuming that the excluded area per head group is similar for subgel and gel DPPC, and the area per chain is slightly smaller for subgel than gel, we argue that the chain tilt is expected to be slightly larger for the subgel phase, as indeed suggested by the electron density profiles.

An interesting finding is that the application of very large applied pressures ($P > 1 \times 10^9$ dyn/cm^2) increases the bilayer thickness for the gel phase but not for the subgel phase. The most likely explanation for the increase in bilayer thickness for the gel phase is a decrease in hydrocarbon chain tilt at high applied pressure for the gel phase. Katsaras et al. (1992) directly observed such a decrease in chain tilt (from 36.6° in excess water to 21.9° at 30% relative humidity) from wide-angle patterns of oriented gel-phase DPPC bilayers. In gel-phase bilayers, factors that decrease the excluded area of the head group relative to the excluded area of the acyl chains also decrease chain tilt (McIntosh, 1980). Removal of water from the head group region of the bilayers by high osmotic pressures decreases the excluded area in the head group region and therefore decreases chain tilt. At such high pressures, steric (excluded volume) interactions between head groups can be partially compensated by increased van der Waals interactions between the acyl chains. Hence, when intercalated water is removed from the head group region, the gel to liquid-crystalline phase transition temperature increases (Simon et al., 1991). The observation that the bilayer thickness remains constant upon dehydration for the subgel phase is consistent with the notion that the subgel phase corresponds to bilayers that are crystalline, and thus incompressible in two dimensions (in the plane of the bilayer), and that pressures as high as several thousand atmospheres are insufficient to remove water intercalated in the head group region. Previously Blaurock and McIntosh (1986) found that the subgel phase of dipalmitoylphosphatidylglycerol did not change in structure over a wide hydration range.

Another difference in the electron density profiles between gel and subgel phases is that the electron density between bilayers is somewhat lower in the subgel phase, even at the highest applied pressures (Figure 5B,C). The profiles are not at high enough resolution to determine unambiguously the reason for this difference. One possibility is that the head group conformation is slightly different in the subgel phase, so that the low electron density methyl groups of the phosphorylcholine group extend slightly farther into the fluid space for subgel than for gel bilayers.

In excess water, the equilibrium fluid separation is about 3 Å larger for the gel phase than the subgel phase (Figure 6A). This result is consistent with the X-ray analyses (Nagle & Wiener, 1988; Ruocco & Shipley, 1982a&b) that found that the gel phase imbibes more water than does the subgel phase. Possible reasons for this observation are examined below.

Pressures between Adjacent Bilayers

The pressure–distance curves for the subgel and the liquid-crystalline phases (Figure 6B) have some important similarities and differences. The data are very similar over a finite range of interbilayer spacings (4 Å $< d_f <$ 8 Å), but differ significantly for $d_f < 4$ Å and $d_f > 8$ Å. These observations imply that molecular motion in the bilayer does not significantly affect the total interbilayer pressure for 4 Å $< d_f <$ 8 Å, but markedly affects the interbilayer pressures for $d_f <$ 4 Å and $d_f > 8$ Å. In addition, the data for subgel bilayers show that over the applied pressure range of 0 to 1×10^9 dyn/cm^2 the interbilayer separation changes only about 5 Å for subgel, compared to about 12 Å for liquid-crystalline phase bilayers (Figure 6A). This implies that long-range entropic interactions, in particular the undulation pressure (Helfrich, 1973; Evans & Parsegian, 1986; Evans & Needham, 1987), have an appreciable influence on the width of the interbilayer fluid space for fluid bilayers. Previously, Evans and Parsegian (1986) had predicted that thermal undulations could displace the minimum energy position to greater interbilayer spacings, as we now experimentally observe.

In order to compare and contrast further the interactions between subgel, gel, and liquid-crystalline bilayers, we have modeled the total pressure–distance relations for these phases in terms of component pressures previously postulated or demonstrated. In this analysis, we assume that the total pressure P between uncharged phosphatidylcholine bilayers can be written as the sum of three repulsive pressures and the

attractive van der Waals pressure. That is,

$$P = P_{vsr} + P_{sr} + P_u - P_v \quad (3)$$

where P_{vsr} represents a very short range steric repulsion between apposing head groups, P_{sr} represents a short range repulsive pressure due to either water orientation (Marcelja & Radic, 1976; Parsegian et al., 1979; Rand & Parsegian, 1989) or molecular protrusions (Israelachvili & Wennerstrom, 1990, 1992), P_u is the repulsive undulation pressure, and P_v is the attractive van der Waals pressure. For these pressures, we use functional forms based on relevant experimental data or theoretical treatments. Thus, we use exponential decays for both P_{vsr} (McIntosh et al., 1987, 1989a) and P_{sr} (Marcelja & Radic, 1976; Parsegian et al., 1979; Rand & Parsegian, 1989; Israelachvili & Wennerstrom, 1990, 1992), such that $P_{vsr} = P_{vsr0}\exp(-d_f/\lambda s)$ and $P_{sr} = P_{sr0}\exp(-d_f/\lambda)$. For the undulation pressure, we use the theoretical expression of Evans and Needham (1987), $P_u = (\pi kT/32\lambda)(P_{sr0}/B\lambda)^{1/2}\exp(-d_f/2\lambda)$, where B is the bilayer bending modulus, and for the van der Waals pressure we set $P_v = -H/6\pi d_f^3$, where H is the Hamaker constant. We note that other functional forms have been postulated for P_u (Helfrich, 1973; Podgornik & Parsegian, 1992). For this analysis we assume that all the pressures refer to the same plane of origin, which we place at the physical edge of the bilayer. We realize that the plane of origin might well be different for each of the component pressures. However, the exact position of the plane of origin is not known precisely for any of the pressures, and we use this simplifying assumption to make the modeling tractable. We emphasize that the numbers obtained for the magnitudes and decay lengths of the various pressures depend on the choice of origin and thus are not uniquely determined by these calculations.

Modeling calculations were performed as described in detail in McIntosh et al., (1989a). The procedure was to fit the total pressure curves in Figure 6 using the functional forms for P_{vsr}, P_{sr}, P_u, and P_v given above. Standard statistical methods (Neter & Wasserman, 1974) were used to obtain a least-squares fit to the pressure data. A Hamaker constant was determined that gave a match between the measured values of the adhesion energy and the energy of adhesion calculated by integrating the total pressure and evaluating at the equilibrium fluid separation. Adhesion energies have been measured as –0.015 erg/cm^2 for egg PC (Evans & Metcalfe, 1984 and –0.15 erg/cm^2 for gel-phase DPPC (Marra & Israelachvili, 1985). We assume that the adhesion energy should be somewhat larger in magnitude for the subgel phase than the gel phase, since the equilibrium fluid separation is smaller in the subgel phase (Figure 6A). We also use the following additional criteria: (1) the energy minima have to be within 1 Å of the equilibrium fluid spacings for each phase, (2) the Hamaker constants for the bilayers in the three phases should be approximately 3×10^{-14} erg (Needham & Haydon, 1983), and (3) the bending modulus B is 10^{-12} erg for liquid-crystalline bilayers (Lorenzen et al., 1986; Servuss & Helfrich, 1987) and is orders of magnitude higher for both the gel and subgel phase, so that $P_u \approx 0$ for the subgel and gel phases.

Since the acyl chain and the head group motions are smaller in the subgel phase than in the gel and fluid phases, we will first analyze the pressures between subgel-phase liquids and use this information as the standard to compare with the pressures between gel and liquid-crystalline phase lipids.

Subgel Phase. The solid line shown in Figure 6A is a fit to eq 3 with $P_{vsr} = 5.18 \times 10^{25}\exp(-d_f/0.07)$ dyn/cm^2, $P_{sr} = 1.11 \times 10^9\exp(-d_f/1.43)$ dyn/cm^2, $P_u = 0$, and $P_v = -3.0 \times 10^{10}/6\pi d_f^3$ dyn/cm^2; $R^2 = 0.99$. The adhesion energy was $E_a = -0.23$ erg/cm^2 at $d_f = 8.5$ Å. The term representing P_{vsr} decreases very rapidly, having a decay length of about 0.07 Å. This steep decay for subgel-phase bilayers reflects an extremely "hard" steric interaction.

The exponential decay for P_{sr} observed for 3 Å < d_f < 8 Å has a magnitude ($P_{sr0} = 1.1 \times 10^9$ dyn/cm^2) and a decay length ($\lambda = 1.4$ Å) that are similar to those previously observed for the pressure between zwitterionic phospholipids in this distance range (McIntosh & Simon, 1986b; Rand & Parsegian, 1989; Simon & McIntosh, 1989; McIntosh et al., 1989a, 1992a). We note that, because the change in fluid space is only about 5 Å for the subgel phase, other functional forms besides an exponential decay could be used for P_{vsr} or P_{sr}. However, an excellent fit to the experimental data was obtained with the expontential decay for these two pressures. The downward break in the pressure–distance relation at $d_f \approx 8$ Å corresponds to the fluid separation where P_{sr} is balanced by the attractive van der Waals pressure.

Comparison of Pressures for Gel and Subgel Phases. Figure 6A shows the pressure–fluid spacing of DPPC in the subgel- and gel-phase bilayers. With regard to the subgel phase, the data points for the gel phase are shifted to higher fluid spacings by approximately 3 Å, with the exception of the three points at the highest pressures. This implies that more work is required to compress gel-phase bilayers than subgel-phase bilayers to $d_f = 3$ Å. The gel-phase data show at least two and possibly three distinct regions in the plot of log P versus d_f: (1) within 11.7 Å ≥ d_f > 11 Å there is only a small increase in d_f with decreasing pressure; (2) within 11 Å > d_f > 6 Å the data points fall near a straight line; and (3) within 6 Å > d_f > 3 Å the data points also fall near a straight line. The first issue is whether or not there is a break at $d_f \approx 6$ Å. That is, the data points for the gel phase can be closely fit with either one or two exponentials representing the repulsive pressure. Thus, the equation $P = 1.66 \times 10^{10}\exp(-d_f/1.21) - (3.0 \times 10^{10})/6\pi d_f^3$ dyn/cm^2, where $E_a = -0.5$ erg/cm^2 at $d_f = 11.5$ Å, represents a good fit to the data ($R^2 = 0.98$). This analysis assumes that the only repulsive pressure present is P_{sr}. However, these data can also be fit well ($R^2 = 0.99$) using two exponential repulsive pressures, P_{vsr} and P_{sr}, so that $P = 7.2 \times 10^{10}\exp(-d_f/0.80) + 4.5 \times 10^9\exp(-d_f/1.40) - (3.0 \times 10^{10})/6\pi d_f^3$ dyn/cm^2, where $E_a = -0.11$ erg/cm^2 at $d_f = 11.9$ Å. The decay constant for P_{sr} is slightly larger for the second case where P_{vsr} is included (1.4 Å compared to 1.2 Å).

Since the fits are both quite good, one cannot distinguish among these two possibilities using curve fitting as the sole criterion. However, there are good reasons to assume the presence of P_{vsr} between gel-phase DPPC bilayers. First, upward breaks in the pressure–distance relations, characteristic of the onset of P_{vsr}, also occur at $d_f \approx 5$–6 Å for bilayers having phosphorylcholine head groups in both the fluid (McIntosh et al., 1987, 1989a) and gel phases (McIntosh et al., 1992a). Second, the simplest explanation for the observation that at the highest applied pressures the fluid spaces for the subgel and gel phases are similar (Figure 6A) is that the motions of the head group in the gel phase have been reduced by entropic confinement to that of the subgel phase. The fact that the upward break in the pressure–distance relation starting at $d_f \approx 5$–6 Å is not nearly as evident in gel-phase DPPC as it is in subgel DPPC (Figure 6A), egg PC (Figure 6B), or sphingomyelin bilayers (McIntosh et al., 1992a) can be explained by the observation that the magnitude of P_{sr} is much greater in gel-phase DPPC than in the other systems. Thus, in the gel phase more work is required to

overcome P_{sr}, and the onset of P_{vsr} is more difficult to distinguish from P_{sr} for DPPC in the gel phase than it is for subgel DPPC, egg PC, or sphingomyelin. Thus, gel-phase DPPC bilayers have P_{sr} with a decay length similar to that of the subgel bilayers. We argue that the fluid spacing of DPPC in the gel phase is greater than that in the subgel phase because the magnitude of P_{sr} is larger in the gel than in the subgel phase.

Comparison of Pressures in Gel and Liquid-Crystalline Phases. The pressure–distance curve extends about 7 Å further for the liquid-crystalline phase than for the subgel phase. The most likely explanation for this difference between subgel and liquid-crystalline phases is the presence of an additional long-range entropic pressure in the liquid-crystalline phase. That such an additional long-range repulsive pressure is present in the fluid phase can be seen from the behavior of the pressure–distance relations for low applied pressures (log $P < 6$). In the gel and subgel phases the fluid spacing changed by about 1 Å on decreasing the applied pressure from 1×10^6 to 0 dyn/cm^2 (figure 6A), whereas in the liquid-crystalline phase the fluid spacing changed by over 5 Å over this pressure range. Therefore, we considered the effects of an additional steric pressure, namely the undulation pressure, to the pressure–distance relation for the liquid-crystalline phase.

The egg PC bilayer data (Figure 6B) were well fit ($R^2 = 0.99$) using the equation $P = P_{vsr} + P_{sr} + P_u - P_v = 7.84 \times 10^{13} \exp(-d_f/0.68) + 4.0 \times 10^8 \exp(-d_f/1.38) + 1.28 \times 10^6 \exp(-d_f/2.76) - 2.5 \times 10^{10}/6\pi d_f^3$ dyn/cm^2 for $E_a = -0.015$ erg/cm^2 at $d_f = 15.4$ Å. Thus, the pressure–distance data for liquid-crystalline egg PC bilayers can be explained in terms of three repulsive pressures, P_{vsr}, P_{sr}, and P_u. The decay length of 1.4 Å found for P_{sr} in the fluid phase is the same as that found for the subgel and gel phases.

Underlying Mechnisms for Component Pressures

Very Short Range Steric Pressure, P_{vsr}. For liquid-crystalline bilayers, there is a rather "soft" upward break in the pressure–distance curve, starting at $d_f \approx 5$–6 Å and extending to $d_f \approx 1.5$ Å with a decay length of about 0.7 Å (Figure 6A). This upward break has been attributed to a very short range steric interaction, P_{vsr}, between the mobile polar head groups that can extend 2–3 Å from each apposing bilayer into the fluid space between bilayers (McIntosh et al., 1987, 1989a). For liquid-crystalline bilayers, molecular protrusions could also contribute to the width of this upward break in the pressure–distance curve (Israelachvili & Wennerstrom, 1992; McIntosh et al., 1992a). In agreement with this pressure being due to steric interactions between head groups due to thermal motion, a recent combined X-ray and neutron diffraction analysis (Wiener & White, 1992) of liquid-crystalline dioleoylphosphatidylcholine bilayers at an applied pressure of 6×10^8 dyn/cm^2 (where we observe P_{vsr}) shows overlap of the distributions of the mobile choline groups from apposing bilayers. Since there is relatively little motion of the lipid molecules in the subgel phase compared to the gel or liquid-crystalline phases, one would expect a sharper upward break in the pressure–distance relations when apposing subgel bilayers come together than when apposing gel or liquid-crystalline bilayers come together. As noted above, we do, in fact, observe an extremely sharp upward break for subgel bilayers (Figures 6A,B), indicating that the sharpness of this upward break, and therefore the range of P_{vsr} depends on head group motion.

There are two unexpected features about the upward break in the pressure–distance curve for subgel bilayer: (1) it occurs at $d_f \approx 3$ Å, rather than at the expected position at $d_f \approx 0$ Å, and (2) the pressure–distance relations for liquid-crystalline and subgel bilayers cross at $d_f \approx 3$ Å (Figure 6B), so that the distance between egg PC bilayers at high applied pressure is smaller than the distance between subgel bilayers. There are several possible factors that could explain why the upward break in the pressure–distance curve for subgel DPPC occurs at $d_f \approx 3$ Å rather than at $d_f \approx 0$ Å. First, experimentally it is difficult to define accurately the edge of the lipid bilayer with moderate resolution (7 Å) electron density profiles (McIntosh & Simon, 1986b; McIntosh et al., 1987, 1989a). Second, our estimate for the water–bilayer interface was made on the basis of the conformation of the PC head group in single crystals, and the conformation of the PC head group might be slightly different in the subgel phase. In particular, we speculate that the head group conformation for subgel DPPC might be crystallized into a conformation such that the PC head group extends into the fluid space an intermediate distance between the maximum and minimum extensions of the head group in both the liquid-crystalline and gel phases. This possibility is consistent with the differences in the electron density profiles for gel and subgel phases (Figure 5C) noted above. Third, water molecules are undoubtedly tightly bound to the polar head group and could extend the range of steric interactions beyond the point of direct interactions between the lipid molecules. That is, the effect of the tightly bound water could be to shift the plane of origin (Israelachvili & Wennerstrom, 1992). Fourth, although the motion of the head group is reduced compared to the motion in gel and liquid-crystalline phases, there still might be some head group motion in the subgel phase that is slow compared to the NMR time scale. The observation that the subgel and liquid-crystalline pressure–distance curves cross can be explained by two possible factors. First, as noted above, the head group in the subgel phase might extend into the fluid space and intermediate distance between the maximum and minimum extensions of the head group in the liquid-crystalline phase. Second, the area per molecule is considerably larger in the liquid-crystalline phase than int he subgel phase (Nagle & Wiener, 1988). Therefore, the liquid-crystalline bilayer is more compressible and deformable than the subgel phase, and at high osmotic pressures the polar head groups of apposing bilayers can probably interpenetrate to a greater extent in the liquid-crystalline phase than they can in the subgel and gel phases. To this point, increasing the spacing between adjacent egg PC bilayers by the addition of equimolar cholesterol eliminates the upward break (McIntosh et al., 1989a).

Short-Range Interaction, P_{sr}. As noted in the introduction, different types of interactions have been postulated to give rise to this exponential decay between neutral bilayers—the partial orientation of water molecules by the bilayer surface (Marcelja & Radic, 1976; Shiby & Ruckenstein, 1983; Dzhavakhidze, 1988; Attard & Batchelor, 1988; Simon & McIntosh, 1989; Leikin & Kornyshev, 1990) and steric (entropic) pressures due to the protrusion of lipid molecules from the bilayer surface (Israelachvili & Wennerstrom, 1990, 1992) or head group flexibility and motion (Granfeldt & Miklavic, 1991; Israelachvili & Wennerstrom, 1992). Our data (Figure 6A,B) show that for 4 Å $< d_f <$ 8 Å, P_{sr} decays exponentially with a decay length of about 1.4 Å for the subgel, gel, and liquid-crystalline phases. Thus, we argue that the same mechanism governs P_{sr} for all three phases. We now consider which of the above possible mechanisms is most consistent with our observed data, keeping in mind Marra and Israelachvili's (1985) discussion about the intimate

coupling of hydration and steric forces. In particular, if the primary hydration shell around each lipid molecule is involved in determining the excluded volume of the head group, then the distinction between hydration and steric interactions becomes somewhat unclear near the boundary between P_{vsr} and P_{sr} at $d_f \approx 4$ Å.

A key observation is that P_{sr} has similar decay length and magnitude for the subgel phase, where the acyl chains are crystallized in two dimensions, and for the liquid-crystalline phase, where the chains have a liquid-like organization in the plane of the bilayer (Figure 6B). This provides evidence that P_{sr} is unlikely to be due solely to molecular protrusions where acyl chains must be exposed to water (Israelachvili & Wennerstrom, 1990, 1992), since the thermal motion of methylene groups should be much smaller for crystalline bilayers than for liquid-crystalline bilayers. For example, the mean displacement of methylene groups in single crystals of lysophosphatidylcholine is only about 0.3 Å (Hauser et al., 1980).

The observation that the magnitude of P_{sr} is larger for gel-phase DPPC than for liquid-crystalline phase egg PC bilayers (Figure 6A,B) or gel-phase sphingomyelin (McIntosh et al., 1992b) provides evidence that P_{sr} represents a pressure primarily due to water reorientation rather than to head group motion or molecular protrusions (McIntosh et al., 1992a). That is, for gel-phase DPPC, liquid-crystalline egg PC, and gel-phase sphingomyelin, the magnitude of P_{sr} is related to the measured dipole potential (Simon & McIntosh, 1989; Simon et al., 1992), which in turn depends on the orientation of water molecules in the head group region (Simon & McIntosh, 1989; Simon et al., 1992; Zheng & Vanderkooi, 1992). If P_{sr} were due to head group motion or molecular protrusions, one would expect its magnitude to be larger for the liquid-crystalline phase than for the gel phase.

The reason the magnitude of P_{sr} is larger for the gel than for the subgel phase is not known. In terms of entropic models, one expects that head group motion and molecular protrusions should be larger for the gel phase compared to the subgel phase. However, the extent of protrusions is unknown and should be quite small for both phases. In terms of a hydration pressure model, as noted above, we have shown for a variety of lipids that the the magnitude of the hydration pressure correlates with the square of the dipole potential measured for monolayers in equilibrium with bilayers (Simon & McIntosh, 1989). Unfortunately, we cannot test this relationship for subgel bilayers. Dipole potentials cannot be measured for the subgel phase since this phase does not form in monolayers and transport studies of lipophilic ions cannot be performed in subgel-phase vesicles.

Therefore, based on comparisons of P_{sr} for subgel, gel, and liquid-crystalline phases (Figure 6A,B), we argue that P_{sr} is due, at least in part, to the reorientation of water molecules. We note, however, that for these three phases the range of d_f where P_{sr} dominates is relatively narrow (about 5–7 Å), meaning that relatively small molecular motions could produce steric contributions for these fluid spacings. Moreover, for the liquid-crystalline phase, P_{sr} lies between two established steric pressures: P_{vsr}, due to protruding headgroups, and P_u, due to thermally induced bending modes. Therefore, the relative contributions of hydration and steric pressures are difficult to demonstrate unequivocally from a single osmotic stress experiment with this lipid phase. A similar situation perhaps also pertains to osmotic stress measurements with other systems, such as DNA helices (Rau et al., 1984; Rau & Parsegian, 1992a,b) or polysaccharide molecules (Rau & Parsegian, 1990). In charged systems, there is the extra complication due to repulsion from electrostatic double layers. In the case of DNA helices, Rau and Parsegian (1992a) have measured the spacing between helices as a function of temperature to investigate the enthalpic and entropic contributions of water in the interaction.

The observation that the decay length for P_{sr} is similar for subgel, gel, and liquid-crystalline bilayers does not seem to be consistent with the theoretical treatments (Kornyshev & Leikin, 1989; Leikin & Kornyshev, 1991; Kornyshev et al., 1992) that predict that the decay length of the hydration pressure should decrease with increasing order in the lipid head group region.

Summary

From the pressure–distance data (Figure 6), it is clear that the interbilayer fluid spacing for subgel bilayers changes only about 5 Å over the entire range of applied pressures. This implies that for this phase the repulsive hydration force has a range of no more than one water molecule beyond the primary hydration shell. The relatively large (15 Å) fluid space for liquid-crystalline bilayers is, at least in part, a consequence of the additional steric undulation pressure.

ACKNOWLEDGMENT

We appreciate several helpful comments on an early draft of this manuscript by Drs. David Needham, Adrian Parsegian, and Jacob Israelachvili, and we thank Dr. Michael Hines for his help with the modeling studies.

REFERENCES

Akutsu, H. (1986) *J. Magn. Reson. 66*, 250–263.
Attard, P., & Batchelor, M. T. (1988) *Chem. Phys. Lett. 149*, 206–211.
Badger, J., & Caspar, D. L. D. (1991) *Proc. Natl. Acad. Sci. U.S.A. 88*, 622–626.
Belaya, M. L., Feigel'man, M. V., & Levadny, V. G. (1986) *Chem. Phys. Lett. 126*, 361–364.
Blaurock, A. E., & Worthington, C. R. (1966) *Biophys. J. 6*, 305–312.
Blaurock, A. E., & McIntosh, T. J. (1986) *Biochemistry 25*, 299–305.
Cevc, G., & Marsh, D. (1985) *Biophys. J. 47*, 21–32.
Chen, S. C., Sturtevant, J. M., & Gaffney, B. J. (1980) *Proc. Natl. Acad. Sci. U.S.A. 77*, 5060–5063.
Dzhavakhidze, P. G., Kornshev, A. A., & Levadny, V. G. (1988) *Il Nuovo Cimento 10D*, 627–654.
Evans, E. (1991) *Langmuir 7*, 1900–1908.
Evans, E., & Metcalfe, M. (1984) *Biophys. J. 46*, 423–426.
Evans, E., & Needham, D. (1987) *J. Phys. Chem. 91*, 4219–4228.
Evans, E. A., & Parsegian, V. A. (1986) *Proc. Natl. Acad. Sci. U.S.A. 83*, 7132–7136.
Fuldner, H. H. (1981) *Biochemistry 20*, 5707–5712.
Gawrisch, K., Arnold, K., Dietze, K., & Schulze, U. (1988) in *Electromagntetic Fields and Biomembranes* (Markov, M., & Blank, M., Eds.) pp 9–18, Plenum Press, New York.
Gawrisch, K., Ruston, D., Zimmerberg, J., Parsegian, V. A., Rand, R. P., & Fuller, N. (1992) *Biophys. J. 61*, 1213–1223.
Grandfeldt, M., & Miklavic, S. (1991) *J. Phys. Chem. 95*, 6351–6360.
Gruen, D. W. R., & Marcelja, S. (1983) *J. Chem. Soc.*, Faraday Trans. *2 79*, 225–242.
Hauser, H., Pascher, I., & Sundel, S. (1980) *J. Mol. Biol. 137*, 249–264.
Helfrich, W. (1973) *Z. Naturforsch 28C*, 693–703.
Herbette, L., Marquardt, J., Scarpa, A., & Blasie, J. K. (1977) *Biophys. J. 20*, 245–272.

Israelachvili, J. N., & Wennerstrom, H. (1990) *Langmuir 6*, 873–876.
Israelachvili, J. N., & Wennerstrom, H. (1992) *J. Phys. Chem. 96*, 520–531.
Katsaras, J., Yang, D. S.-C., & Epand, R. M. (1992) *Biophys. J. 63*, 1170–1175.
Kornyshev, A. A. (1986) *J. Electroanal. Chem. 204*, 79–84.
Kornyshev, A. A., & Leikin, S. (1989) *Phys. Rev. A 40*, 6431–6437.
Kornyshev, A. A., Kossakowski, D. A., & Leikin, S. (1992) *J. Chem. Phys. 97*, 6809–6820.
Leikin, S., & Kornyshev, A. A. (1990) *J. Chem. Phys. 92*, 6890–6898.
Leikin, S., & Kornyshev, A. A. (1991) *Phys. Rev. A 44*, 1156–1168.
LeNeveu, D. M., Rand, R. P., & Parsegian, V. A. (1976) *Nature 259*, 601–603.
LeNeveu, D. M., Rand, R. P., Parsegian, V. A., & Gingell, D. (1977) *Biophys. J. 18*, 209–230.
Lesslauer, W., Cain, J. E., & Blasie, J. K. (1972) *Proc. Natl. Acad. Sci. U.S.A. 69*, 1499–1503.
Lis, L. J., McAlister, M., Fuller, N., Rand, R. P., & Parsegian, V. A. (1982) *Biophys. J. 37*, 657–666.
Lorenzen, S., Servuss, R.-M., & Helfrich, W. (1986) *Biophys. J. 50*, 565–572.
Marcelja, S., & Radic, N. (1976) *Chem. Phys. Lett. 42*, 129–130.
Marra, J., & Israelachvili, J. (1985) *Biochemistry 24*, 4608–4618.
McIntosh, T. J. (1980) *Biophys. J. 29*, 237–246.
McIntosh, T. J., & Simon, S. A. (1986a) *Biochemistry 25*, 4948–4952.
McIntosh, T. J., & Simon, S. A. (1986b) *Biochemistry 25*, 4058–4066.
McIntosh, T. J., & Holloway, P. W. (1987) *Biochemistry 26*, 1783–1788.
McIntosh, T. J., Magid, A. D., & Simon, S. A. (1987) *Biochemistry 26*, 7325–7332.
McIntosh, T. J., Magid, A. D., & Simon, S. A. (1989a) *Biochemistry 28*, 17–25.
McIntosh, T. J., Magid, A. D., & Simon, S. A. (1989b) *Biochemistry 28*, 7904–7912.
McIntosh, T. J., Magid, A. D., & Simon, S. A. (1989c) *Biophys. J. 55*, 897–904.
McIntosh, T. J., Simon, S. A., Needham, D., & Huang, C.-h. (1992a) *Biochemistry 31*, 2020–2024.
McIntosh, T. J., Simon, S. A., Needham, D., & Huang, C.-h. (1992b) *Biochemistry 31*, 2012–2020.
Nagle, J. F., & Wiener, M. C. (1988) *Biochim. Biophys. Acta 942*, 1–10.
Needham, D., & Haydon, D. A. (1983) *Biophys. J. 41*, 251–258.
Neter, J., & Wasserman, W. (1974) *Book Applied Linear Statistics*, p 228, R. D. Irwin, Homewood, IL.
O'Brien, F. E. M. (1948) *J. Sci. Instrum. 25*, 73–76.
Parsegian, V. A., & Rand, R. P. (1991) *Langmuir 7*, 1299–1301.
Parsegian, V. A., Fuller, N., & Rand, R. P. (1979) *Proc. Natl. Acad. Sci. U.S.A. 76*, 2750–2754.
Pearson, R. H., & Pascher, I. (1979) *Nature 281*, 499–501.
Podgornik, R., & Parsegian, V. A. (1992) *Langmuir 8*, 557–562.
Raghavan, K., Rami Reddy, M., & Berkowitz, M. L. (1992) *Langmuir 8*, 233–240.
Rand, R. P., & Parsegian, V. A. (1989) *Biochim. Biophys. Acta 988*, 351–376.
Rau, D. C., & Parsegian, V. A. (1990) *Science 249*, 1278–1281.
Rau, D. C., & Parsegian, V. A. (1992a) *Biophys. J. 61*, 260–271.
Rau, D. C., & Parsegian, V. A. (1992b) *Biophys. J. 61*, 246–259.
Rau, D. C., Lee, B., & Parsegian, V. A. (1984) *Proc. Natl. Acad. Sci. U.S.A. 81*, 2612–2625.
Ruocco, M. J., & Shipley, G. G. (1982a) *Biochim. Biophys. Acta 684*, 59–66.
Ruocco, M. J., & Shipley, G. G. (1982b) *Biochim. Biophys. Acta 691*, 309–320.
Safinya, C. R., Sirota, E. B., Roux, D., & Smith, G. S. (1989) *Phys. Rev. Lett. 62*, 1134–1137.
Schiby, D., & Ruckenstein, E. (1983) *Chem. Phys. Lett. 95*, 435–438.
Servuss, R. M., & Helfrich, W. (1987) in *Physics of Complex and Supermolecular Fluids* (Safran, S. A., & Clark, N. A., Eds.) pp 85–100, Wiley, New York.
Shannon, C. E. (1949) *Proc. Inst. Radio Eng., N.Y. 37*, 10–21.
Simon, S. A., & McIntosh, T. J. (1989) *Proc. Natl. Acad. Sci. U.S.A. 86*, 9263–9267.
Simon, S. A., McIntosh, T. J., & Latorre, R. (1982) *Science 216*, 65–67.
Simon, S. A., McIntosh, T. J., & Magid, A. D. (1988) *J. Colloid Interface Sci. 126*, 74–83.
Simon, S. A., Fink, C. A., Kenworthy, A. K., & McIntosh, T. J. (1991) *Biophys. J. 59*, 538–546.
Simon, S. A., McIntosh, T. J., Magid, A. D., & Needham, D. (1992) *Biophys. J. 61*, 786–799.
Tardieu, A., Luzzati, V., & Reman, F. C. (1973) *J. Mol. Biol. 75*, 711–733.
Tristam-Nagle, S., Wiener, M. C., Yang, C.-P., & Nagle, J. F. (1987) *Biochemistry 26*, 4288–4294.
Vink, H. (1971) *Eur. Polym. J. 7*, 1411–1419.
Weast, R. C. (1984) *Handbook of Chemistry and Physics*, CRC Press, Boca Raton, FL.
Wiener, M. C., & White, S. H. (1992) *Biophys. J. 61*, 434–447.
Worcester, D. L., & Franks, N. P. (1976) *J. Mol. Biol. 100*, 359–378.
Zheng, C., & Vanderkooi, G. (1992) *Biophys. J. 63*, 935–941.